

# **Study of Josephson Junction**

## **Simulations and analysis**

Submitted in partial fulfillment of the requirements of

*BITS F421T Thesis*

*By*

Ashwin Kumar K

ID No. 2017B5A81034G

*Under the guidance of :*

Dr. Kartik Senapati, NISER, Bhubaneswar

&

Dr. Ramesha C K, BITS Pilani, Goa

May 10, 2022



## **Declaration**

I, Ashwin Kumar K, declare that this Undergraduate Thesis titled, ‘Study of Josephson Junction - Simulations and analysis’ and the work presented in it are my own. I confirm that:

- This work was done mainly or wholly while in candidature for a research degree at this University.
- Where any part of this thesis has previously been submitted for a degree or any other qualification at this University or any other institution, this has been clearly stated.
- Where I have consulted the published work of others, this is always clearly attributed.
- Where I have quoted from the work of others, the source is always given. With the exception of such quotations, this thesis is entirely my own work.
- Where the thesis is based on work done by myself jointly with others, I have made clear exactly what was done by others and what I have contributed myself.
- I have acknowledged all main sources of help.

Signed:

Date:

## Acknowledgments

I wish to thank my project supervisors, Dr. Kartikeswar Senapati and Dr. Ramesha C K for their immense support and help with the understanding of this project. I would like to express my deepest appreciation to Mr. Tapas Ranjan Senapati and Ms. Laxmipriya Nanda for all their help from mentoring on the fabrication techniques to usage of measurement systems and all the fruitful discussions. I wish to thank all the lab members of Superconductivity lab, NISER for all the brainstorming sessions which helped me greatly. Special thanks to Ms. Soheli Mukherjee who always supported me with all my endeavors. I would also like to extend my deepest gratitude to Dr. Dhavala Suri who always showered me with helpful advice. Lastly, I am thankful to all my friends and family members for extending their love and support.

# Contents

<b>I</b>	<b>Introduction</b>	<b>7</b>
<b>1</b>	<b>Superconductivity</b>	<b>7</b>
<b>2</b>	<b>Josephson Junctions</b>	<b>8</b>
2.1	RCSJ model . . . . .	9
2.2	Josephson Junctions in the Presence of a Magnetic Field . . . . .	12
<b>II</b>	<b>Simulation Details</b>	<b>14</b>
<b>3</b>	<b>Modeling the ODE</b>	<b>14</b>
<b>4</b>	<b>Simulation parameters</b>	<b>15</b>
<b>5</b>	<b>Simulation Results</b>	<b>17</b>
5.1	Experimental Measurements . . . . .	23
5.2	Comparing simulation with experimental data . . . . .	29
<b>6</b>	<b>Processing experimental data</b>	<b>29</b>
6.1	Automation of $I_c$ extraction . . . . .	29
6.2	Inferring $I_c$ behavior via repetitive IV measurement . . . . .	31
<b>7</b>	<b>Conclusion</b>	<b>35</b>
	<b>References</b>	<b>37</b>

## Abbreviations

- AC :- Alternating current
- RF :- Radio frequency
- JJ :- Josephson Junction
- SQUID :- Superconducting QUantum Interference Device
- EDX :- Energy Dispersive X-ray spectroscopy
- SEM :- Scanning Electron Microscope
- FIB :- Focused Ion Beam
- PPMS :- Physical Properties Measurement System
- Fig :- Figure
- eV :- Electron Volt
- KeV :- Kilo Electron Volt
- MeV :- Mega/Million Electron Volt
- et al :- And others (Latin)
- i.e. :- That is
- etc :- Et cetera (Latin for 'and others of same kind')
- T :- Tesla
- SiO<sub>2</sub>:- Silicon dioxide
- R-T :- Resistance Versus Temperature
- I-V :- Current Versus Voltage
- I-H :- Current Versus Magnetic field
- V-H :- Voltage Versus Magnetic field
- Si :- Silicon
- K :- kelvin
- mm :- millimeter
- mbar :- millibar
- IPA :- Isopropyl alcohol
- RPM :- Revolutions Per Minute

- C :- Celsius
- Ar :- Argon
- e.g. :- Example given
- TSP :- Titanium Sublimation Pump
- RGA :- Residual Gas Analyzers
- Cu :- Copper
- BCS :- Bardeen–Cooper–Schrieffer
- Nb :- Niobium
- DC :- Direct current
- AC :- Alternating current
- $\mu\text{A}$  :- Micro Ampere
- $\Omega$ :- Ohm
- nm :- Nano meter

# Part I

## Introduction

At the beginning of this thesis, we introduce basic theoretical concepts that underlay the device we are trying to study, i.e. the Josephson Junction (JJ). We first study the postulates of superconductivity. Then we look at the Josephson effect, which describes the physics of a Superconductor-Insulator-Superconductor sandwich and then look at a popular model of a realistic Josephson junction, namely the RCSJ model. Later we will try to understand various aspects of fabrication and characterisation of such devices.

### 1 Superconductivity

Heike Kamerlingh Onnes discovered the phenomenon of superconductivity in the Netherlands in 1911. He was the first to observe that the electrical resistance becomes exactly zero in certain materials and in temperatures below a specific critical value  $T_c$  [1]. Soon after this discovery, several other materials that showed superconducting behaviour were discovered, with different critical temperatures. Currently the highest temperature at which superconductivity was observed is in hydrogen sulphide ( $H_2S$ ), which has a  $T_c$  reported as 203K, but at extremely high pressures [2]. In 1933, Meissner and Ochsenfeld discovered that within a superconductor, the magnetic field completely vanishes i.r becomes zero, making the superconductor a perfect diamagnet. The expulsion of a magnetic field inside a superconductor is called the Meissner effect. Then the London brothers explained this effect, who proved that the magnetic field inside a superconductor has an exponential decay from the surface, with a decay length  $\lambda$ , called London penetration depth. They explained that in order to facilitate this, the superconductor sets up electric currents on its surface, whose magnetic field opposes and cancels the applied magnetic field within the superconductor. The phenomenon of superconductivity was theoretically explained in 1957, almost 46 years after its initial discovery, by Bardeen, Cooper, and Schrieffer [3]. They proposed the first microscopic theory of superconductivity, which was named the BCS theory, and received the Nobel Prize in Physics in 1972. They suggested that the electrons of a superconductor that are close to the Fermi surface attract indirectly through the crystal lattice, which is mediated by the exchange of phonons. This attraction overcomes the Coulomb repulsion between the two electrons and the electrons form pairs, which we now call as Cooper pairs. Cooper pairs feel no scattering, and thus lead to the formation of supercurrent. In  $T > T_c$  though, the thermal vibration energy of the lattice becomes more significant than the pairing energy of the electrons, so the Cooper pair breaks, and thus the material becomes normal. It was later discovered that superconducting materials behave in different ways upon application of external magnetic fields. There are two major categories of superconductors which are type I and type II. A type I has only one critical field (keeping other parameters

like current density and temperature constant) above which all superconductor properties are lost and while in superconducting state all magnetic field lines or magnetic flux are completely pushed out from the bulk of the material. In the case of a type II superconductor, there exists two separate critical field values between which a single flux quanta,  $\phi_0$ , of the magnetic field is allowed to pass through the superconductor through isolated points and are called vortices. Currently one of the most used applications of superconductivity is to produce extremely high magnetic fields ranging into tens of teslas can trace it's origin back to 1955 when G. B. Yntema created the first ever superconducting electromagnet using superconducting Nb wire windings with an iron-core, this setup was outputting a 0.7 T magnetic field

## 2 Josephson Junctions

Prior to 1962, researchers were familiar with quantum mechanical tunnelling of normal electrons through a weak barrier; however, the probability of tunnelling of a cooper pair was thought to be insignificant given that the pair as a whole would have to tunnel through the barrier. In 1962 Brian David Josephson showed that this tunnelling probability is not low as previously thought. He predicted theoretically that two superconductors that are coupled (are in close proximity) by a weak link, which link may be made of a normal metal, an insulator, or a constriction of superconductivity, can still let the supercurrent flow through them [4]. This macroscopic phenomenon was given the name Josephson effect.

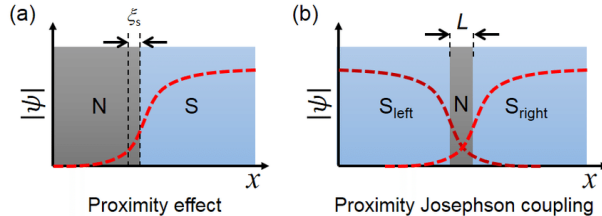


Figure 1: (a) The superconducting order parameter  $\Psi$  of a superconductor (S) penetrating into the normal metal (N) with a length scale of the superconducting coherence length,  $\xi$ . (b) Order parameters from two sides have an overlap in N, producing proximity Josephson coupling.[5]

Josephson demonstrated that, for a short junction, the current that flows through the junction when no voltage bias is applied, and the phase difference  $\phi$  across the junction, which is the difference in the phase factor between the order parameter of the two superconductors, are related through the relation:

$$I_s = I_c \sin(\delta) \quad (1)$$

Here,  $I_c$  is the supercurrent amplitude and  $\delta = \phi_1 - \phi_2$ , where  $\phi_i$  is the phase of

each superconductor. This phenomenon is known as the DC Josephson effect. Josephson also showed AC Josephson effect where an applied constant voltage bias  $V$  on the junction leads to sinusoidal oscillations in the junction current and is governed by the equation:

$$V = (\Phi_0/2\pi) \dot{\delta} \quad (2)$$

where  $\Phi_0 \approx 2 \times 10^{-15}$  Weber is the flux quantum.

The DC Josephson effect is explained by a process known as Andreev reflection [1]. A.F.Andreev explained the phenomenon in 1964 establishing the concept of the so-called Andreev reflection. This reflection occurs at the interfaces between the superconductor S and a normal metal N. Andreev suggested that an electron that approaches the interface from the normal metal side can travel through the superconductor side by the formation of a Cooper pair with another electron with opposite momentum and spin on the superconductor side. At the same time, reflect a hole inside the normal metal region thus balancing the charge. As a result of this cycle, a pair of correlated electrons is transferred from one superconductor to another, creating a supercurrent flow across the junction. It explains how a normal current in the normal metal side becomes a supercurrent in the superconductor side. The AC Josephson relation in essence suggests that a Josephson junction can be a perfect voltage-to-frequency converter. The inverse is also possible by using a microwave frequency to induce a DC voltage in a Josephson junction, this phenomena is known as inverse AC Josephson effect.

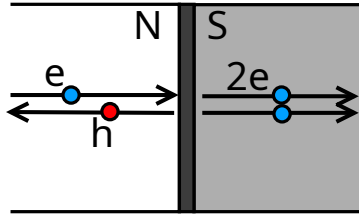


Figure 2: Andreev Reflection process

## 2.1 RCSJ model

A Josephson junction, is typically composed of two superconducting electrodes separated by weaklink which is typically insulating, thus such a junction would have some unavoidable capacitance  $C$  (Just like the parallel plate capacitor separated by a dielectric). If the junction current exceeds the critical current of the junction then quasi-particle excitations are generated. These quasi-particle currents are not superconducting and can be quite lossy just like a normal metal current, so we represent this as a normal resistor  $R$ . This gives us the resistively and capacitively shunted junction (RCSJ) model. This model helps us simulate

the characteristics of a Josephson junction. A schematic representation of the same can be seen in Fig 3.

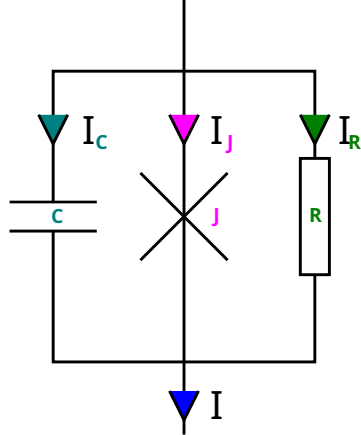


Figure 3: A schematic representation of RCSJ model. Here  $I$  is the current through the device,  $I_c$  is the current through the capacitor  $I_J$  is the current through the Josephson Junction,  $I_R$  is the current through the resistance

Writing out Kirchov's circuit laws for the RCSJ model (from Fig 3.) we can find

$$I_c + I_J + I_R = I$$

$$\frac{\Phi_0}{2\pi} C \ddot{\delta} + I_c \sin(\delta) + \frac{\Phi_0}{2\pi R} \dot{\delta} = I$$

or

$$\frac{\Phi_0}{2\pi} C \ddot{\delta} + \frac{\Phi_0}{2\pi R} \dot{\delta} = I - I_c \sin(\delta)$$

Rearranging as

$$\ddot{\delta} + \frac{1}{RC} \dot{\delta} = \left( \frac{2\pi}{C\Phi_0} \right) (I - I_c \sin(\delta)) \quad (3)$$

we can interpret Eq 3 as the dynamics of a damped particle with the following physical properties:

$$\text{"effective mass"} = C$$

$$\text{"coefficient of friction"} = 1/R$$

$$\text{"potential experienced by the particle"} = -(2\pi/C\Phi_0) (I\delta + I_c \cos(\delta)).$$

The dynamics of the Josephson junction phase difference in-terms of the damped particle can be described as follows: (Fig 4)

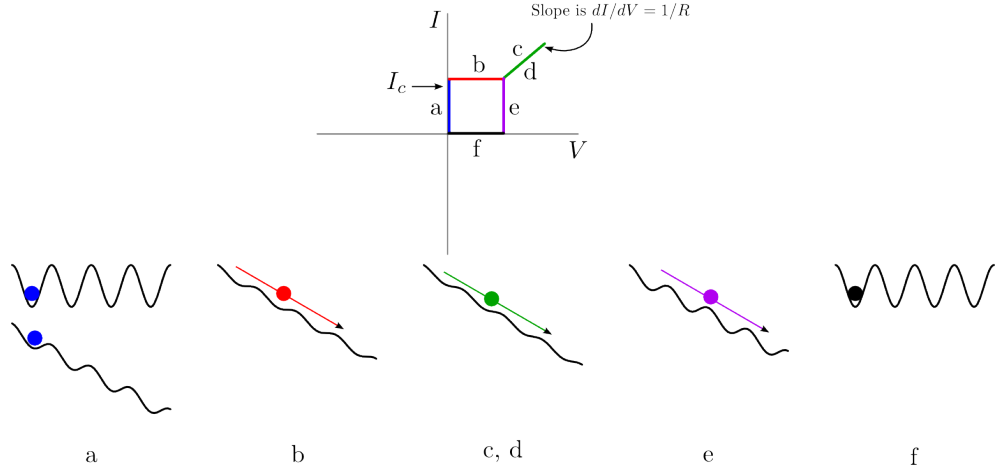


Figure 4: Interpretation of the washboard potential[6]

- The junction has a simple cosine potential when there is no junction current (at  $I=0$ ). At this point, the pseudo-particle is caught in one of the cosine's wells, as shown in Fig 4a. We can observe the effect of an extra linear term to the potential as we introduce some current. Because the potential now resembles a tilted washboard, it's known as the *tilted washboard potential*. There are still vallies in the potential if the bias current is less than  $I_c$ , and the ball remains stuck, as shown in Fig 4a. Because the junction phase (i.e the pseudo-particle) is stuck at a fixed value of  $\delta$ , the voltage is zero (as  $V \propto \delta$ ). As demonstrated by the horizontal blue line, this is the section of the IV curve where an increase in junction current does not result in an increase in junction voltage. Because the junction element is still superconducting, all current flows through the tunnel element and none through the resistor at this point, resulting in the junction.
- As the current is increased past  $I_c$ , the linear term in the potential begins to dominate the cosine part, and the vallies fade away. As demonstrated in Fig 4b the junction pseudo particle then rolls downhill. The pseudo particle is now in a time-varying phase, and the junction voltage is non-zero and approaches a finite value, as shown by the red line in Fig 4b
- Because the current  $I$  now exceeds the tunnelling element's critical current, the tunnelling element no longer acts as a superconductor. The formation of quasiparticles makes the connection resistive. In other words, the resistive element carries practically all of the current. Further increases in current result in a linear increase in voltage, identical to that of a typical metal, as indicated by  $V = IR$ , as shown in Fig 4c, and by the green line marked Fig 4c.

- As the current is reduced, we return to the green line, as shown by the mark Fig 4d. The rest of the process depends on how fast we are raising and lowering the current. The potential regains its cosine nature and regains vallies, as we lower the current below  $I_c$ .
- If there were no dissipative forces as is the case when we sweep fast enough or when whatever dissipation remains can't completely stop the particle, the particle would continue to roll down as it already has energy. Therefore, even as I is lowered below  $I_c$  we still have time varying  $\delta$  and therefore still have a measurable voltage. This can be concluded from Fig 4e and the pink line in Fig 4e
- In the end, we go back to no bias case where the potential is again a cosine term and as we slowly sweep the voltage we slow down and finally stop the particle. Then as we increase the negative bias the process starts all over in reverse.

## 2.2 Josephson Junctions in the Presence of a Magnetic Field

In Eq1 we saw that the Josephson Junction current depends on the phase difference  $\delta$  across the junction. When an external magnetic field is applied, the field influences the phase difference  $\delta$ , this in turn causes interesting dynamics between the Josephson Junction current and the applied external magnetic fields. It can be shown that in the case of a small Josephson Junction this dependence follows the relation[1]:

$$I_J = I_0 \left| \frac{\sin\left(\pi \frac{\Phi_J}{\Phi_0}\right)}{\pi \frac{\Phi_J}{\Phi_0}} \right|$$

here  $\Phi_J = \mu_0 H w (d + \lambda_1 + \lambda_2)$  is the magnetic flux linked to the whole barrier with  $w$  being the width of the barrier,  $d$  the barrier thickness,  $\lambda_1, \lambda_2$ , the penetration depths of the two superconductors.

This behavior was first experimentally found by Rodwel [7], in a Pb-I-Pb junction at 1.3 K. This is the standard form of the Fraunhofer pattern  $F(x) = I_0 \sin^2(\pi x)/(\pi x)^2$  and is seen as a unique characteristic confirmation of a Josephson junctions. This Fraunhofer-like result, which is akin to diffraction of monochromatic, coherent light passing through a slit, provides a validation of the sinusoidal current phase relation (CPR).

For a SQUID, the critical current-magnetic field characteristic is similar to that of Josephson Junctions with the addition of SQUID oscillations superimposed on it. Both of these signatures are in the simulations done in the later section. In case of junctions with ferromagnetic behavior, at certain temperature and barrier width, a  $\pi$ junctions could be observed. This is due to exchange field-induced oscillations of the order parameter and is very sensitive to the temperature and the ferromagnetic layer thickness. In such materials the CPR could

be written as  $I(\phi) = I_0 \sin(\phi + \pi)$ , and doubling of periodicity in  $I_c$  vs  $H$  is observed[8]. In materials with broken time-reversal and broken parity symmetries (this can be obtained in systems with both a Zeeman field and a Rashba spin-orbit coupling[9, 10]), the CPR could take the form of  $I(\phi) = I_0 \sin(\phi + \phi_0)$  [9], in Josephson junctions this term leads to the anomalous phase shift, which could manifest as the presence of second harmonics in the critical current - phase relation [11]. This system is also simulated as a part of the thesis, where in the  $I_C H$  behavior is replaced with the following:

$$I_c = I_{c1} \left| \frac{\sin \left( \pi \frac{\Phi_J}{\Phi_0} \right)}{\pi \frac{\Phi_J}{\Phi_0}} \right| \quad \text{first harmonics} \quad (4)$$

$$I_c = I_{c1} \left| \frac{\sin \left( \pi \frac{\Phi_J}{\Phi_0} \right)}{\pi \frac{\Phi_J}{\Phi_0}} \right| + I_{c2} \left| \frac{\sin \left( 2\pi \frac{\Phi_J}{\Phi_0} \right)}{2\pi \frac{\Phi_J}{\Phi_0}} \right| \quad \text{with second harmonics}$$

## Part II

# Simulation Details

The characteristic signature of a Josephson junction, apart from its current voltage relation (IV) is the Critical current  $I_c$  dependence on the applied magnetic field  $H$  (  $I_C$  vs  $H$  or  $I_C H$  ).

The PPMS in the lab has builtin recipes only for DC measurement and as such DC measurements like IV are relatively slower (1 IV scan in 10-15 minutes on good resolution). Thus getting data for  $I_c H$  would require multiple IVs to be measured at a sweep of magnetic field  $H$ . This would take almost a day per device on a decent resolution and thus cant be done frequently. The more easier measurement would be to set and constant current (say the  $I_c$  at zero magnetic field) then measure the Voltage as a function of changing magnetic field ( V vs  $H$  or  $VH$  ) however, there is little literature regarding the characteristics of  $VH$  relation (or magneto resistance ) of a Josephson junction.

Thus the main goal of the thesis is to verify the correlation between the  $I_C H$  and  $VH$  signatures of a Josephson junction via simulation. simulation part of the thesis is to first setup the numerical solution to the ODE 3 , then simulate an I - V measurement, Iterate the IV sweep over multiple magnetic fields linearly spaced between  $-2\frac{\phi}{\phi_0}$  and  $2\frac{\phi}{\phi_0}$  . This would give us the data of all permissible sets junction current  $I_J$ ,junction voltage  $V_J$  and the applied magnetic field  $H$  that are the possible states of the given Josephson Junction. Finally, one could correlate the simulation with experimental data for junctions with and without second harmonics from  $I_c H$  and  $VH$  measurements. First lets us try to understand the systems ODE.

### 3 Modeling the ODE

We model the Josephson junction using the RCSJ model as described in sec2.1:he total current running through the network is

$$I(t) = I_s(t) + I_R(t) + I_C(t) \quad (5)$$

$$I(t) = I_c \sin(\phi) + \frac{V}{R} + C \frac{dV}{dt} \quad (6)$$

$$V(t) = \frac{\hbar}{2e} \frac{d\phi}{dt}, \frac{dV}{dt} = \frac{\hbar}{2e} \frac{d^2\phi}{dt^2} \quad (7)$$

$$\rightarrow I(t) = I_c \sin(\phi) + \frac{\hbar}{2eR} \frac{d\phi}{dt} + \frac{\hbar C}{2e} \frac{d^2\phi}{dt^2} \quad (8)$$

Due to quasiparticle tunnelling, the resistance in reality relies on both the temperature and the voltage across the junction as described by this equation:

$$R(V, T) = \begin{cases} R_{sg}(T) & \text{for } |V| \leq 2\Delta(T)/e \\ R_n & \text{for } |V| \geq 2\Delta(T)/e \end{cases} \quad (9)$$

where typically  $R_{sg} \gg R_n$ . The characteristic voltage of the junction is accordingly defined as  $V_c = I_c R_n$ .

The current-phase relation (CPR)  $I_s(t) = I_c \sin(\phi)$  describes the supercurrent via a Josephson junction (JJ), where  $I_c$  is the critical current and  $\phi$  is the junction phase-difference. The CPR can be stated in more broad terms as [12, 13]

$$I_s(t) = \sum_{n \geq 1} I_{c_n} \sin(n\phi)$$

, and when the first harmonic is suppressed (for example, at a  $0 - \pi$  transition)[14], the second harmonic may become apparent. We try to determine the influence of adding a second harmonic CPR in the I c H and V H behavior in this thesis by simulation.

Before we try to solve the ODE 8, we can try to simplify the ODE by normalising the equation.

This helps in minimizing the round off errors, for instance if one variable has the value 24582 (units a) the other variable could be in the order 0.001861(units b). The significance of the second variable could be irreversibly lost while executing any operation pertinent to these variables, such as multiplication. One technique to assist limit these possible losses is to normalise the variables first. The equation is simplified with normalized time ( unitless ) via the plasma frequency,  $\tau = \omega_p t$  where  $\omega_p = (2eI_{c0}/\hbar C)^{1/2}$ :[1]

$\omega_p = \frac{1}{\tau_p} = \frac{1}{\sqrt{I_c C}} = \sqrt{\frac{2eI_c}{\hbar C}}$  and  $dt = \frac{1}{\omega_p} d\tau \rightarrow \frac{d^n}{dt} = \omega_p^n \frac{d^n}{d\tau}$ , applying these factors we get

$$\begin{aligned} \frac{I}{I_c} - \sin(\phi) &= \underbrace{\frac{\hbar}{2eI_c R} \sqrt{\frac{2eI_c}{\hbar C}}}_{\sqrt{\frac{\hbar C}{2eI_c R C}} \equiv Q^{-1}} \frac{\phi}{\tau} + \underbrace{\frac{\hbar C}{2eI_c} \frac{2eI_c}{\hbar C}}_1 \frac{d^2\phi}{d\tau^2} \\ \implies \frac{d^2\phi}{d\tau^2} &= \frac{I}{I_c} - \sin(\phi) - \frac{1}{Q} \frac{d\phi}{d\tau} \end{aligned} \quad (10)$$

In this eq 10 Q is the damping factor (or quality factor) which depends on the inherent resistive and capacitive components of the RCSJ model. This Q is identical with  $\beta_c^{1/2}$ , where  $\beta_c$  is a frequently used damping parameter that was introduced by Stewart and McCumber. In the case of heavy damping ( $Q \ll 1$ ) we see the same IV behavior for increasing and decreasing current, however in the case of under damped junction ( $Q \gg 1$ ), while decreasing the current, we see that the junction remains in the non zero voltage range below  $I_c$ . This behavior is also explored in the simulations.

The  $I_c$  in eq 10, is the critical current and its dependence with magnetic field is to be incorporated separately in the simulation based on Eq 4.

## 4 Simulation parameters

The ODE 10 can be converted to a system of first order ordinary differential equations, and then it can be passed on to a ODE solver like `scipy.integrate.odeint`

with the initial values.

$$\begin{aligned} \dot{y}_0 &= \frac{d\phi}{d\tau} \quad \text{with } y_0 = \phi \\ \dot{y}_1 &= \frac{I}{L_c} - \sin(\phi) - \frac{y_0}{Q} \quad \text{with } y_1 = \dot{\phi} \end{aligned}$$

The result one such ODE solve is  $\phi$  and  $\dot{\phi}$  as a function of time for the given initial conditions of  $\phi$ ,  $\dot{\phi}$  and  $I$ . The dynamics of such a system depend vastly on the initial condition given to the ODE. As an example consider the ODE solution as a function of time (in  $\tau$ ) for different initial conditions for  $\phi$  and  $\dot{\phi}$  in Fig 5.

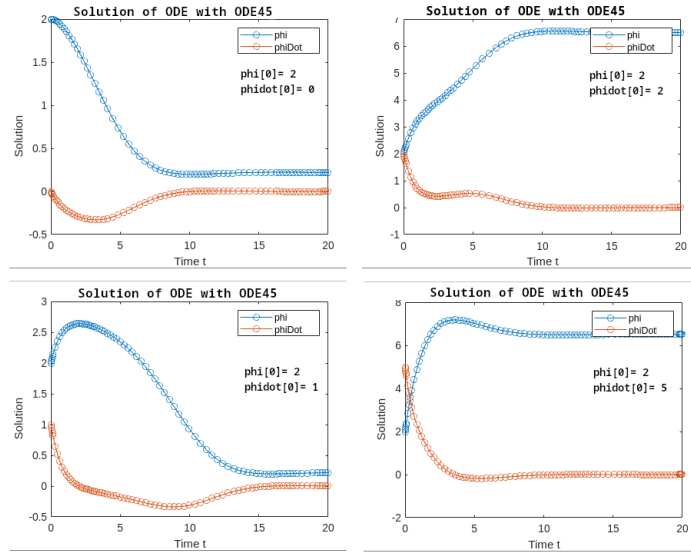


Figure 5: ODE solution as a function of time (in  $\tau$ ) for different initial conditions for  $\phi$  and  $\dot{\phi}$

For the first iteration of the simulation (0 current and 0 phase difference) starting point for  $\phi$  and  $\dot{\phi}$  should be set to zero as any  $\dot{\phi}$  would have to start from the moment a superconducting phase sets up and gradually evolves with time to reach equilibrium.

After the system evolves for a certain amount of time steps (which needs to be adjusted depending on  $Q$ ), the voltage is calculated by averaging over the last cycle (detected as a percentage of the entire time solve). If there's no voltage cycle, the voltage gets set to zero. The initial condition for the next run (next current value in the IV sweep) is the final state of that previous one.

The percentage of final cycle and the number of cycles to be run is determined

for each range of  $Q$  (below 0.1, below 1 below 10, below 100) and kept in a function called *timeparams*.

The entire process is then iterated over the given range of given currents. It must be noted that since the simulation for current depends on the previous relaxed values for  $\phi$  and  $\dot{\phi}$ , the voltage values for a given  $I$  depend on whether the current is a part of the increasing I cycle or decreasing I cycle. Thus one could clearly differentiate between the over damped IV and under damped IV based on the presence of re-trapping current. See fig 6. In the case of heavy damping ( $Q \ll 1$ ) we see the same IV behavior for increasing and decreasing current, however in the case of under damped junction ( $Q \gg 1$ ), while decreasing the current, we see that the junction remains in the non zero voltage range below  $I_c$ .

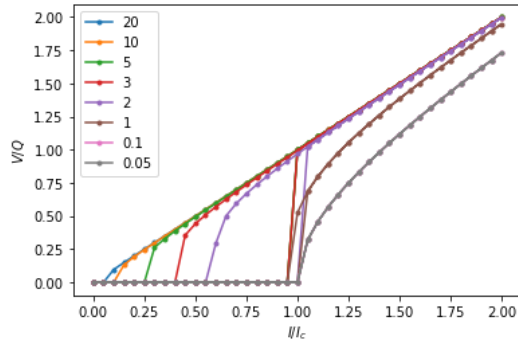


Figure 6: IV sweep (both cycles) for selected under damped and over damped  $Q$ 's. Low damping ( $Q \gg 1$ ) results in substantial hysteresis with an almost linear retrapping branch, whereas the IV for high damping ( $Q \ll 1$ ) is without any hysteresis.

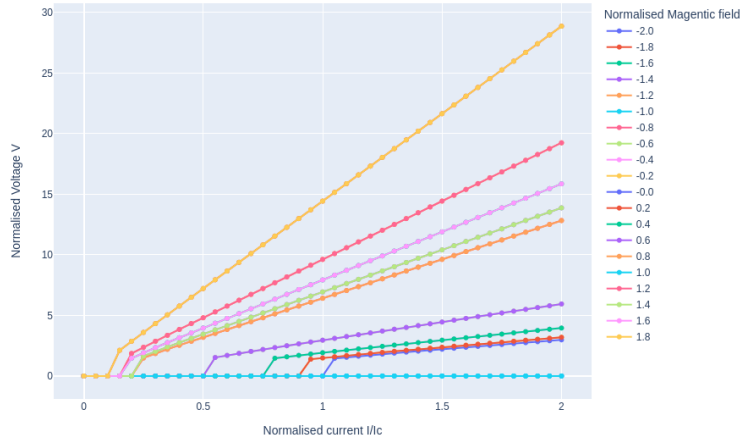
The overall architecture for setting up the simulation including several functions have been referenced from [15].

## 5 Simulation Results

After plotting the IV sweeps for various  $Q$  as in Fig 6, it was found out that  $Q$  value between 1 and 5 has the closest resemblance to experimental IV. Thus all further simulation were made with  $Q=1.5$  and  $Q=0.5$  for checking the over damped and under damped cases.

Plots of the simulations are showing in Fig7 & 8.

I V for different values of H with Q=1.5 including 1st harmonics



I V for different values of H with Q=1.5 including 2nd harmonics

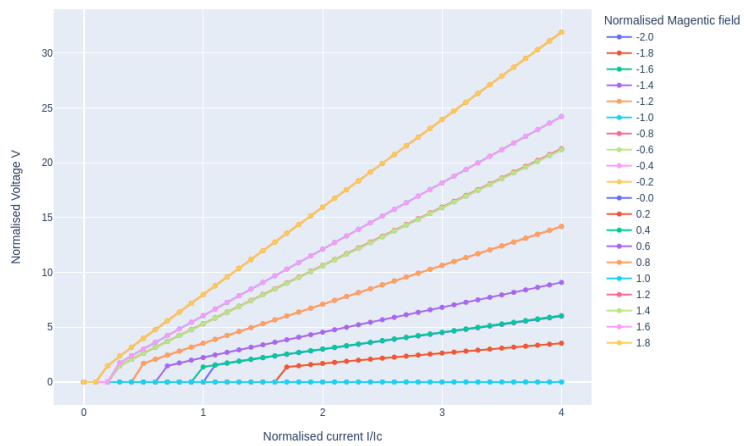
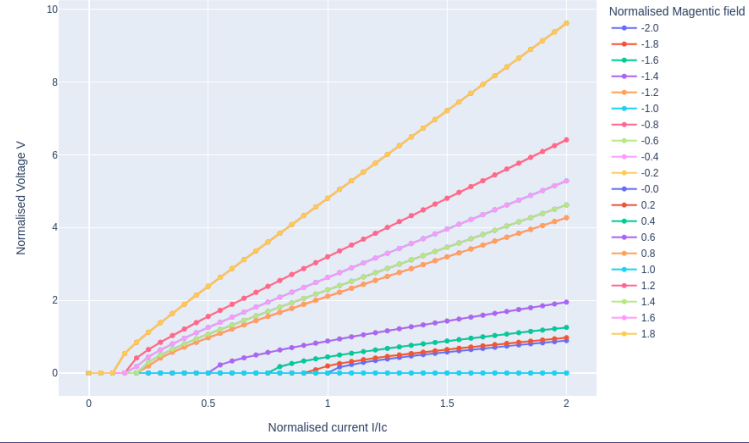


Figure 7: Plots of  $IV$  for simulation with parameter  $Q=1.5$  (under damped) and only first harmonics (top) and with second harmonics (bottom)

I V for different values of H with Q=0.5 including 1st harmonics



I V for different values of H with Q=0.5 including 2nd harmonics

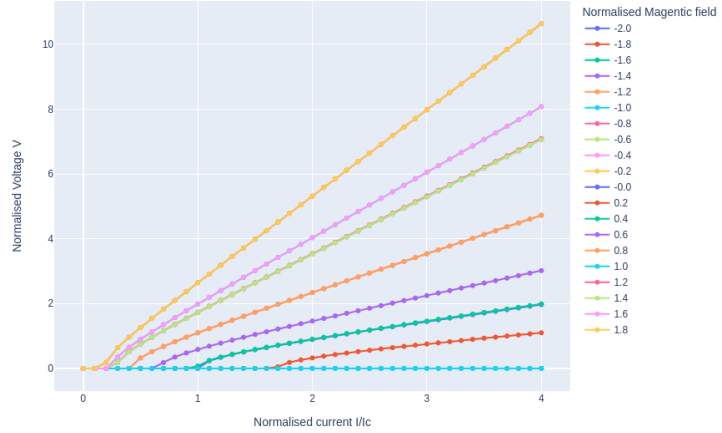


Figure 8: Plots of  $IV$  for simulation with parameter  $Q=0.5$  (over damped) and only first harmonics (top) and with second harmonics (bottom)

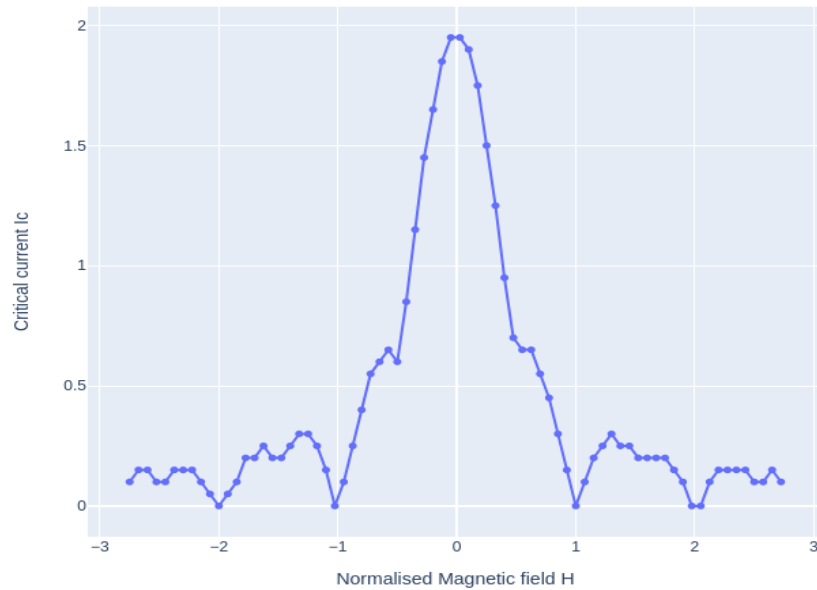
In the case of heavy damping ( $Q = 0.5$ ) we see the same IV behavior for increasing and decreasing current, however in the case of under damped junction ( $Q = 1.5$ ), while decreasing the current, we see that the junction remains in the non zero voltage range below  $I_c$  which is as expected. The variation in the  $I_c$  as a function of applied magnetic field  $H$  is also evident.

The next part of the analysis is to compute the  $I_C H$  data and  $VH$  data from these simulations in both the first harmonics case as well as the second harmonics case.

In Fig9, we see the plots of  $I_cH$  (top) and log plot of  $VH$  (bottom) from simulation with parameter  $Q=1.5$  and second harmonics enabled. The  $I_cH$  and  $VH$  plots have similar shape at the key magnetic field points. ie the main lobe width and the side lobe widths are same. The characteristic second harmonic kinks appear at the same positions as well thus confirming the hypothesis that  $I_cH$  and  $VH$  (magnetoresistance) have similar characteristics for a Josephson junction. Fig 10 is the same plots of  $I_cH$  and  $VH$  for  $Q=1.5$  but with only the first harmonics included. Here too the  $I_cH$  and  $VH$  (magnetoresistance) have similar characteristics further confirming the hypothesis.

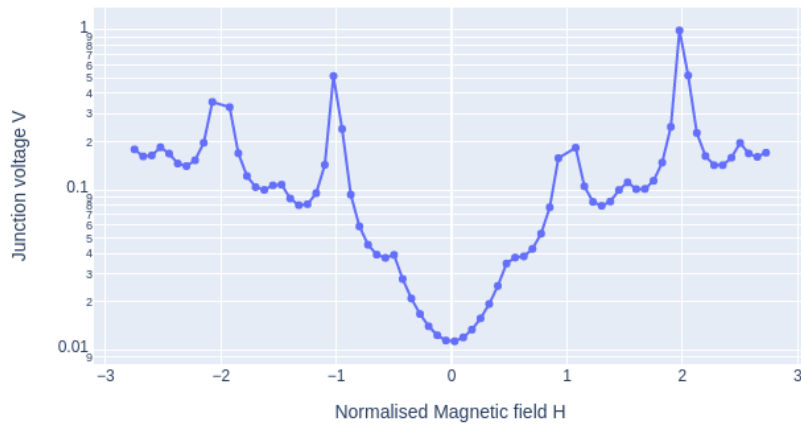
---

I<sub>c</sub> for different values of H for Q=1.5\_2nd-harmonics



---

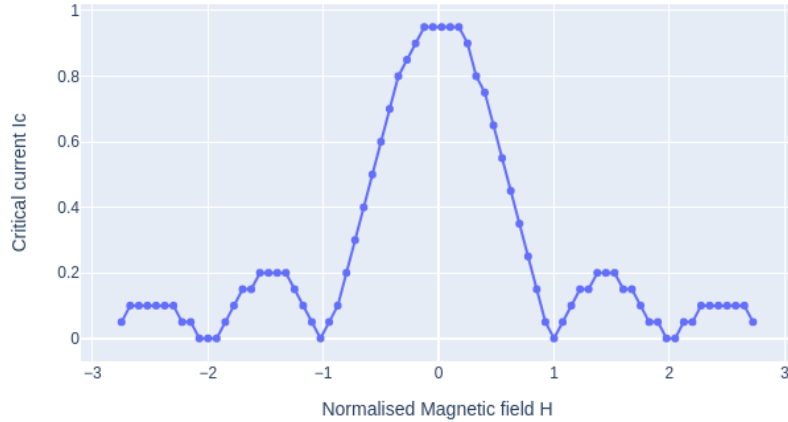
V for different values of H for Q=1.5\_2nd-harmonics



---

Figure 9: Plots of  $I_cH$  (top) and  $VH$  (bottom) from simulation with parameter  $Q=1.5$  and second harmonics added

$I_c$  for different values of  $H$  for  $Q=1.5$ \_1st-harmonics



$V$  for different values of  $H$  for  $Q=1.5$ \_1st-harmonics

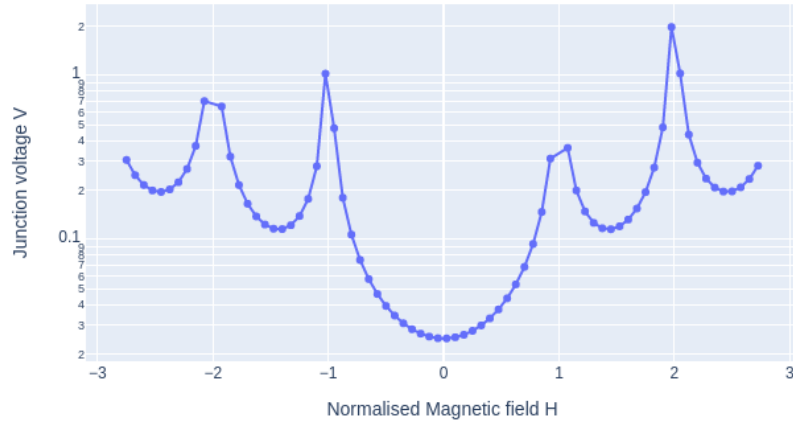


Figure 10: Plots of  $I_cH$  (top) and  $VH$  (bottom) from simulation with parameter  $Q=1.5$  and only first harmonics being kept

One must notice that the  $VH$  plots in bot the above figures have y axis in log scale. The reason for this is that for the selected  $Q=1.5$  the junction resistance turns out to be extreamly large at  $120\Omega$ , the typical resistnace of a junction lies in the milli ohm range, thus the reported Voltages for the same current would

be magnitudes higher, thus a log plot is taken inorder to correct this.

$V$  for different values of  $H$  for  $Q=1.5$ \_2nd-harmonics

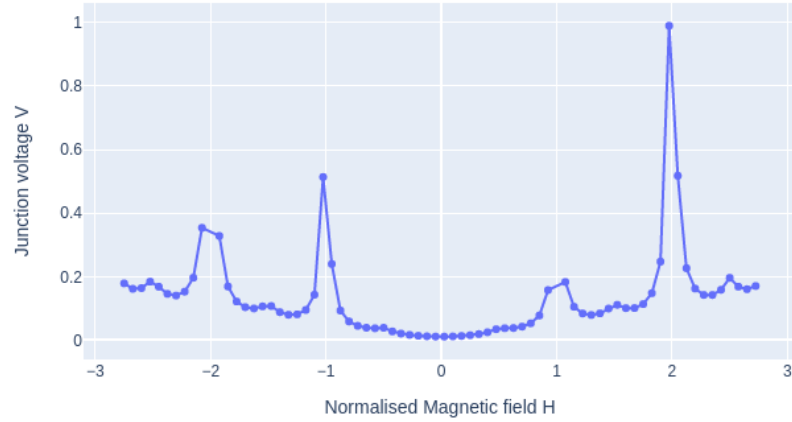


Figure 11: Plots of  $VH$  from simulation with parameter  $Q=1.5$  and y-axis not log normalised

### 5.1 Experimental Measurements

There are two geometries in which the Josephson junction are fabricated using FIB, one is the vertical Junction (Fig 13), and the other is the planar Junction (Fig 12); both names describe the path the current takes through the trilayers. In the planar Junction, the current is in plane with the trilayers and in the case of the vertical junctions the current flows vertically through the trilayers.

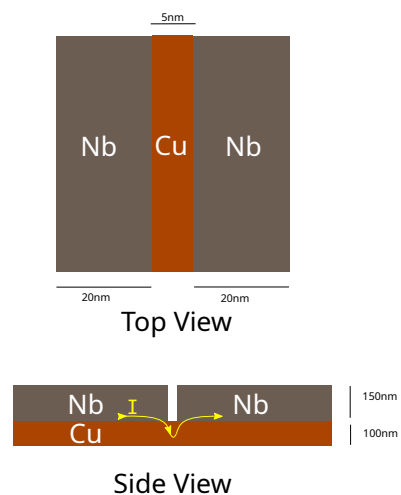


Figure 12: Schematic of the Planar Josephson Junction, due the vertical FIB cut in the Niobium layer, the current travels in plane through first the Niobium layer then through the copper weaklink then finally through the other Niobium layer. The yellow arrowed line shows the direction of current flow

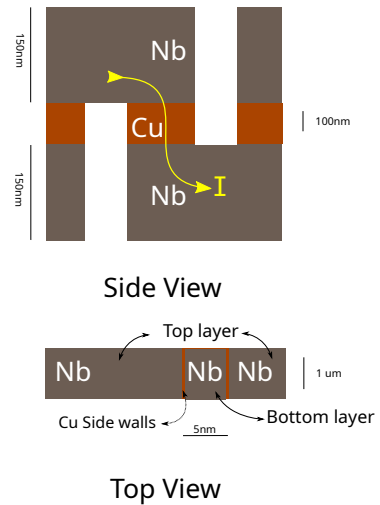


Figure 13: Schematic of the Vertical Josephson Junction, due to the nano pillar cuts on the left and the right, the current travels in plane through first the top Niobium layer then through the copper weaklink then finally through the other Niobium layer. The yellow arrowed line shows the direction of current flow

All the superconducting devices were first cooled to sub 2K, and then a 4 probe resistance vs temperature measurement was carried out with  $1 - 10 \mu\text{A}$  by ramping the temperature slowly to 10K, in order to see the phase transitions. One such R-T graph is shown in Fig 14.

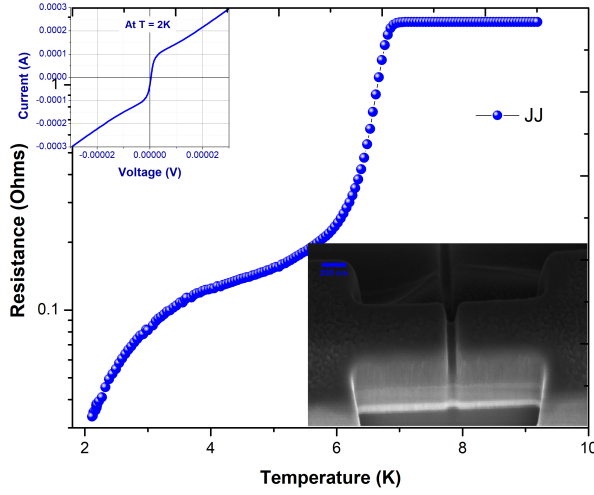


Figure 14: RT graph for a Cu(100nm)Nb(150nm) Josephson junction. The inset shows an SEM image of the measured JJ

The first transition indicates the superconducting transition of the Niobium layer, and the second transition explains the proximitisation of the weak link. The resistance  $R_n$  at 9K (above  $T_c$ ) and  $R_L$  at 2K are noted and the sample is cooled back to sub 2K.  $R_n$  is the normal resistance and indicates that the device is out of the superconducting regime. Once the devices cool down to 2K the current-voltage characteristics of the device is measured by sweeping current from  $-I_n$  to  $+I_n$ , where  $I_n$  is the current for which the device yields the resistance  $R_n$  at 2K, ie. the device switches to the normal regime. The I-V curves have the typical JJ behavior and is plotted in Fig 15.

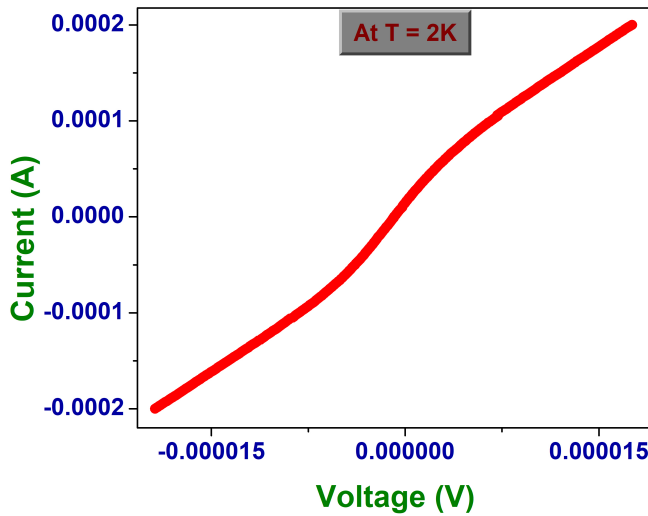


Figure 15: IV graph for a Cu(100nm)Nb(150nm) Josephson junction

$I_c$  of the device and the electrodes were extracted using the python scripts mentioned in section 6.1.

In Fig 15 the IV curve of a Nb/Cu Josephson Junction is shown. Once the device  $I_c$  is found, the device is cooled to 2K and then supplied with  $I_c$  current, and the junction voltage is measured while ramping the magnetic field from +250 Oe to -250 Oe ( positive cycle ) and then from -250Oe to 250Oe ( negative cycle ) at 2K. This gives us magnetoresistance as a function of the applied magnetic field. The magnetoresistance as a function of applied magnetic field is expected to have a diffraction pattern for JJ. This was explained in the theoretical sections above.

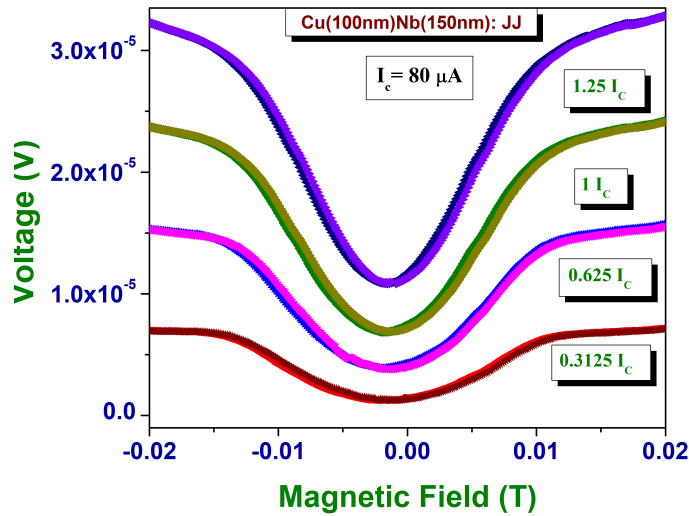


Figure 16: Magnetoresistance of the patterned Nb/Cu Josephson junction device in low magnetic fields for different values of junction currents

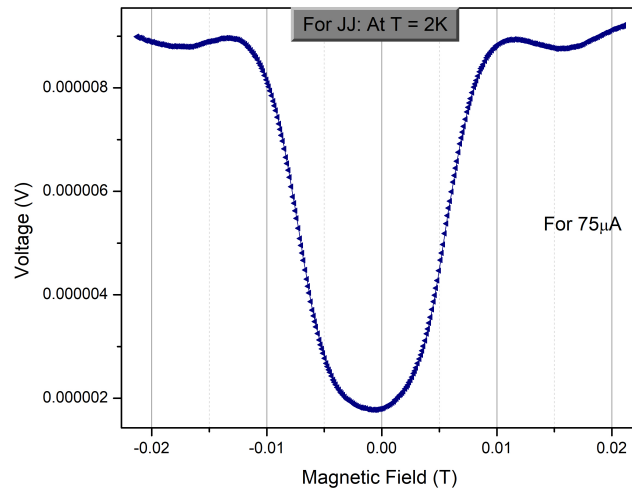


Figure 17: Magnetoresistance of the patterned Nb/Cu Josephson junction device in low magnetic fields

In Fig 17 , we examine the magnetoresistance of the patterned Nb/Cu Josephson junction device in low magnetic fields ( $|H| < 300$  Oe) and at its  $I_c$ . We find that the main lobe of the positive and the negative cycle overlap completely and there is no shift of the main lobe from origin as one would expect for a normal S-N-S junction. Fig 17 is a plot of Junction voltage as a function of magnetic field for another patterned Nb/Cu Josephson junction device in low magnetic fields for different values of junction currents. One can observe that higher currents increase the height of the lobes however the ratio of the first (main) lobe to the second lobe remains constant. This pattern was also confirmed with the simulation results.

## 5.2 Comparing simulation with experimental data

In Fig 17. Magnetoresistance of the patterned Nb/Cu Josephson junction device (which exhibits first harmonics only) in low magnetic fields for different values of junction currents is plotted. This plot is similar to the  $VH$  plot obtained from the simulation for  $Q=1.5$  with only first harmonics enabled (Fig 10 (bottom) ). This further confirms the equivalence between  $VH$  plot obtained experimentally and  $VH$  plot obtained from simulations, Thus establishing that the  $VH$  plot obtained experientally confirms the typical characteristic of the Josephson junction.

# 6 Processing experimental data

## 6.1 Automation of $I_c$ extraction

Once the IV simulation is done, in order to aggregate data for  $I_c$  as a function of applied magnetic field  $H$  ( $I_c H$ ) and Junction voltage at as a function of applied magnetic field  $H$  ( $VH$ ), One must first set the process for identifying  $I_c$ . In case of simulations, since the data is quite smooth, we could choose a junction voltage which corresponds to  $I_c$  for one run and find the current value for that particular voltage on other runs. This is essentially a horizontal slice of the IV curve in Fig 6. For experimental data, there is another way to define the  $I_c$  of a given PPMS data.

$I_c$  of the junction were extracted from this data by running through a python script that takes in the I-V data, calculates  $dV/dI$ , and applies a Savitzky–Golay filter of first-order to obtain  $d^2I/d^2V$  and find the current ( $I_c$ ) for which  $d^2I/d^2V$  in both the positive and negative side and averages them. For normal Josephson junction the position of peak of  $dI/dV$  is a good marker of the  $I_c$ , however in cases where the junction resistance is high,  $dI/dV$  might not be clear enough to mitigate this peaks of  $d^2I/d^2V$  is a better marker of  $I_c$  A sample graph of  $dI/dV$  and  $d^2I/d^2V$  for a I vs V curve measured on a Josephson junction is shown in Fig 18.

Plot for  $dV/dI$  and its derivative



Figure 18: A sample graph of  $dI/dV$  and  $d^2I/d^2V$  for a I vs V curve measured on a Josephson junction. The  $I_c$  extracted from the graph is  $140\mu A$

The code for the python script is available here and a web app based on the same is hosted at [jj-ic-finder.herokuapp.com](http://jj-ic-finder.herokuapp.com)

The web app also provides quick access to multiple data visualizations like area plot, bar plot, line plot, hist plot, scatter plot etc. A screenshot of the web-app in use for visualizing the IV of an experimental data of JJ is shown in Fig19.

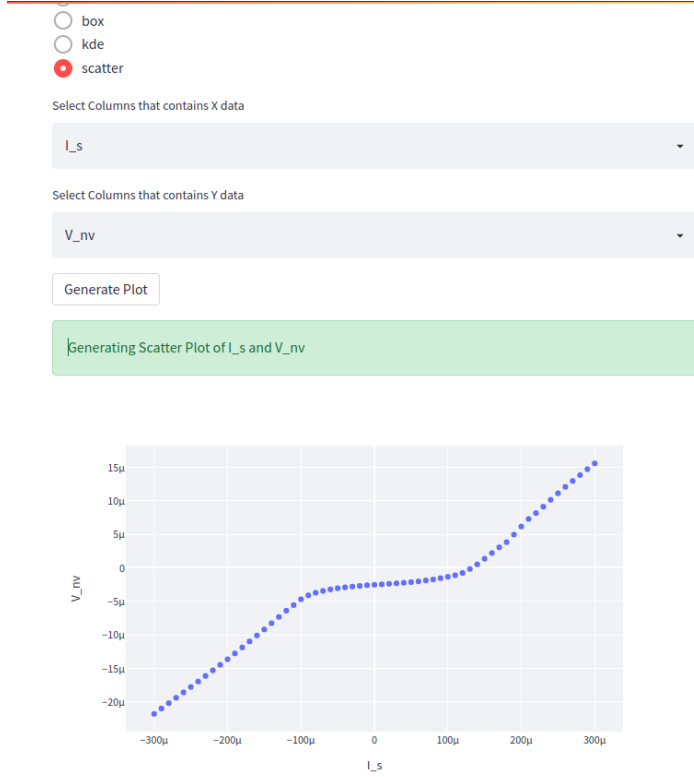


Figure 19: A screenshot of the web-app in use for visualizing the scatter plot of Josephson junctions IV

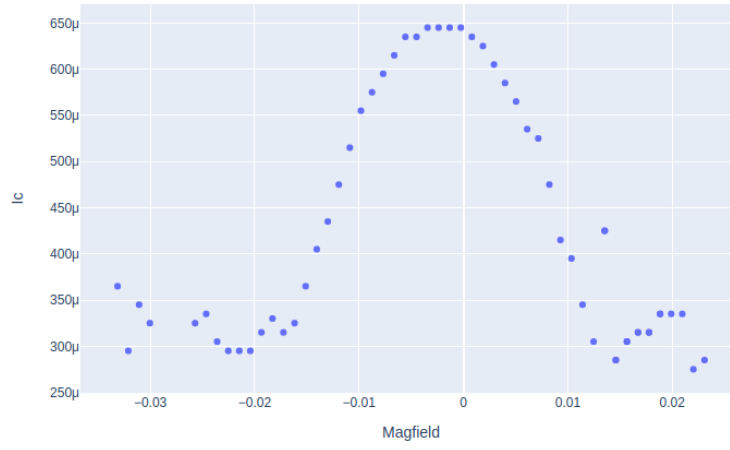
## 6.2 Inferring $I_c$ behavior via repetitive IV measurement

The characteristic signature of a Josephson junction, apart from its current voltage relation (IV) is the Critical current  $I_c$  dependence on the applied magnetic field H ( $I_C$  vs H or  $I_C H$ ).

The PPMS in the lab has builtin recipes only for DC measurement and as such DC measurements like IV are relatively slower (1 IV scan in 10-15 minutes on good resolution). Thus getting data for  $I_c H$  would require multiple IVs to be measured at a sweep of magnetic field H. This would take almost a day per device on a decent resolution and thus cant be done frequently. The more easier measurement would be to set and constant current (say the  $I_c$  at zero magnetic field) then measure the Voltage as a function of changing magnetic field ( V vs H or VH ) however, there is little literature regarding the VH relation (or magneto resistance) of a Josephson junction. In order to verify the correlation between the  $I_C H$  and VH signatures of a Josephson junction, apart from the simulation methods, multiple IV seeps of a Josephson Junction were setup at varying magnetic field were taken, and a python script mentioned in the previous

sub section was used to identify the  $I_C$  for each  $H$ . The plots of these  $I_C H$  and  $VH$  data is shown in Fig . The VH data for these junctions have some parts which are offset due to random phase jumps. On comparison, one can make out the Fraunhofer like pattern in both plots at the same magnetic field points, the main lobe width and the secondary lobe width are identical.

IcH for SP169 JJ4 Pt20nm Voltage selector mode



VH for SP169 JJ4 Pt20nm

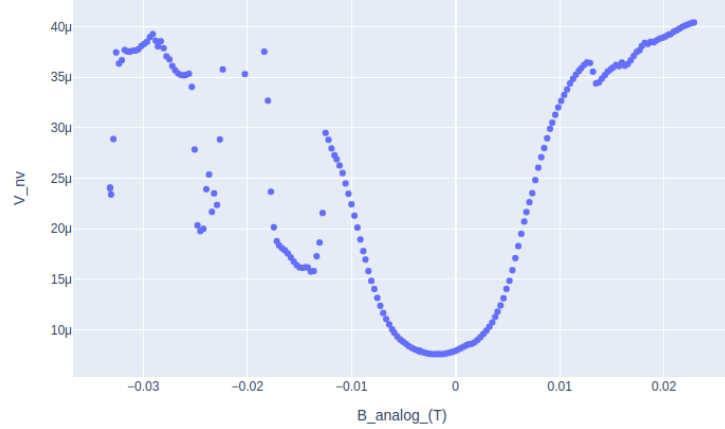
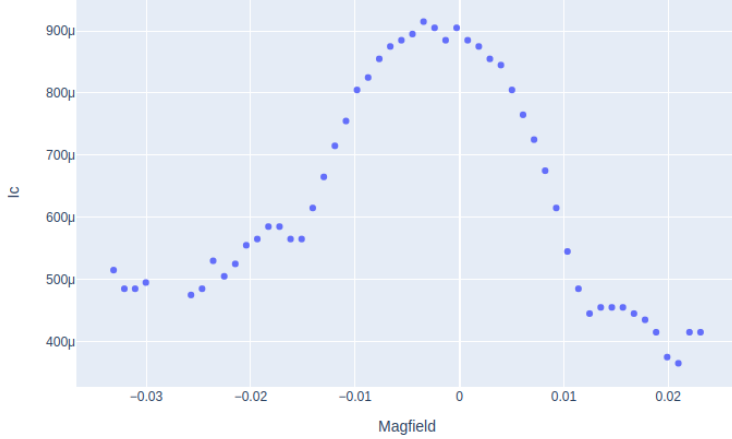


Figure 20: Plots of  $I_C H$  (analyzed from data) and  $VH$ (directly measured) for a Niobium/Copper/Platinum Josephson junction (Sample no 4 from run SP169) One can make out the Fraunhofer like pattern in both plots at the same magnetic field points.

IcH for SP169 JJ5 Pt20nm Voltage selector mode@8.47e-6 V



VH for SP169 JJ5 Pt20nm

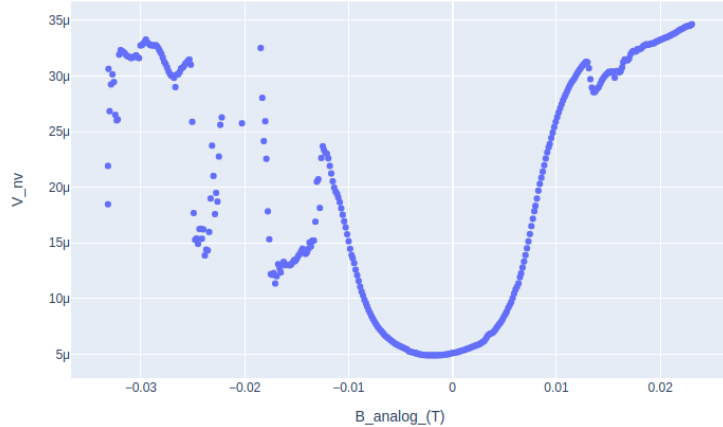


Figure 21: Plots of  $I_c H$  (analyzed from data) and  $VH$ (directly measured) for a Niobium/Copper/Platinum Josephson junction (Sample no 5 from run SP169) One can make out the Fraunhofer like pattern in both plots at the same magnetic field points.

Apart from this measurement, an attempt was made to setup Keithley 6221 - AC current source and Keithley 2182a - Nanovoltmeter in differential conductance mode.

This method involves sweeping a linear staircase profile with an alternating current. The differential current,  $dI$ , is the amplitude of the alternating portion of the current as shown in Fig 22. Throughout the test, the differential current

remains constant. A Trigger Link cable synchronises the current source with the nanovoltmeter. The nanovoltmeter calculates the delta voltage between consecutive steps after measuring the voltage at each current step. To determine the differential voltage,  $dV$ , each delta voltage is averaged with the previous delta voltage.  $dI/dV$  may now be used to calculate the differential conductance,  $dG$ . [16]

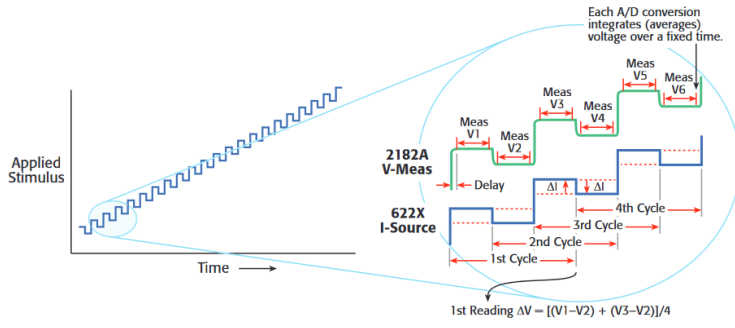


Figure 6a. Applied current during Keithley Differential Conductance measurement

Figure 6b. Detail of applied current and measured device voltage

Figure 22: A plot of the applied current bias in the differential conductance setup[16]

The Labview program provided by the instrument manufacturer required the connection to the 6221 via a GPIB interface, however the 6221 was connected to a system with no GPIB port. In order to overcome this, communication was setup serially via the Ethernet ports and python serial communication library. A graphical user interface (GUI) was built to control the communication and perform the differential conductance as shown in Fig 23.

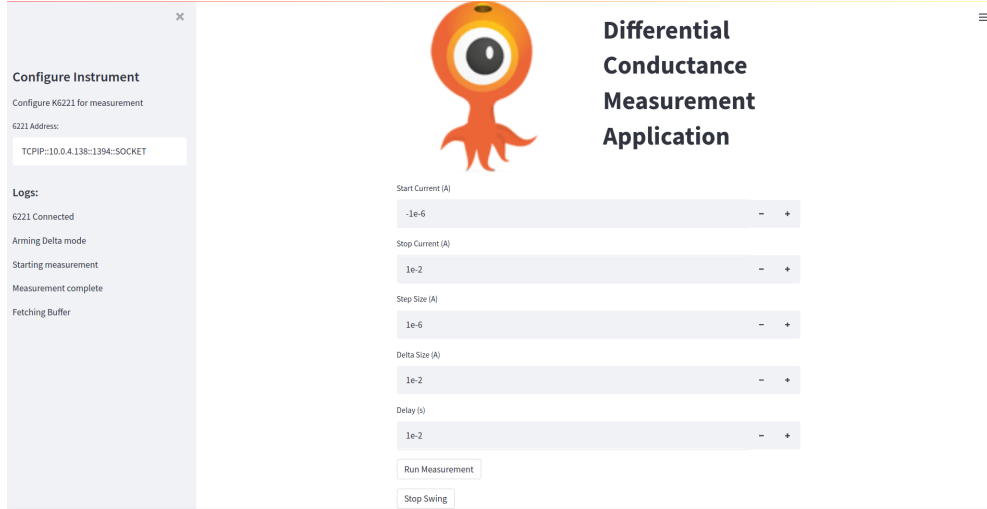


Figure 23: A GUI setup to control the differential conductance setup

The data provided by the instrument is differential conductance,  $dG$  as a function of applied current. The experiment needed  $dG$  as a function of junction voltage and the data acquired by the device was quite unreliable and noisy, thus this method was not used further. A better way to do differential conductance would be to use a lock-in amplifier.

## 7 Conclusion

The main goal of the thesis was to establish equivalence between the  $I_cH$  and  $VH$  (magnetoresistance) characteristics of a Josephson junction (with and without the second harmonics), then further establish the experimental  $VH$  plot and the simulated  $VH$  plot.

For the first part, the simulation was setup by solving the ODE with input similar to the experimental input of, sweeping the current while equilibrating the system at each step and then repeatig this over multiple magnetic field, then further analysing this data to obtain  $I_cH$  and  $VH$  plots. For the second part, experimental data was gathered similar to the simulation steps (calculating IV data for multiple magentic field ) and then analysed to to obtain  $I_cH$  and  $VH$  plots, the results obtained from this was matched with the simulation results.

In both of the above method, the equivalence between the  $I_cH$  and  $VH$  (magnetoresistance) characteristics of a Josephson junction was confirmed and was also matched with the experimental results. One could carry out the study further by:

- Carrying out a simulation analysis with respect to  $\beta_c$ and compare it with the results obtained through Q

- Simulation of other exotic CPR such as  $\sin(\phi/2)$
- The simulation currently takes about 2hrs for sweeping magnetic fields linearly spaced between  $-2\frac{\phi}{\phi_0}$  and  $2\frac{\phi}{\phi_0}$ . An improvement in the simulation/integration time by using numba decorators for numpy-python modules could be made, for instance Scipy's odeint integration will be slow if the right-hand side of an ODE integration is slow. The numba package, which translates python code into machine code using LLVM - which means it's very fast, it can speed up the right-hand side. Even a very simple ODE can be sped up by several factors.
- A study could be done on finding the Q value of the experimental junction, by fitting the IV with Q as a parameter
- The differential conductance measurement could be setup using a lockin amplifier.

## References

- [1] J. R. Schrieffer and M. Tinkham, “Superconductivity,” *Rev. Mod. Phys.*, vol. 71, pp. S313–S317, Mar 1999.
- [2] A. P. Drozdov, M. I. Eremets, I. A. Troyan, V. Ksenofontov, and S. I. Shylin, “Conventional superconductivity at 203 kelvin at high pressures in the sulfur hydride system,” *Nature*, vol. 525, pp. 73–76, Aug. 2015.
- [3] J. Bardeen, L. N. Cooper, and J. R. Schrieffer, “Theory of superconductivity,” *Phys. Rev.*, vol. 108, pp. 1175–1204, Dec 1957.
- [4] B. Josephson, “Possible new effects in superconductive tunnelling,” *Physics Letters*, vol. 1, no. 7, pp. 251–253, 1962.
- [5] G.-H. Lee and H.-J. Lee, “Proximity coupling in superconductor-graphene heterostructures,” *Reports on Progress in Physics*, vol. 81, p. 056502, mar 2018.
- [6] DanielSank, “What does the  $i$ - $v$  curve in josephson junction mean?.” Physics Stack Exchange. URL:<https://physics.stackexchange.com/q/197150> (version: 2015-08-02).
- [7] J. M. Rowell, “Magnetic field dependence of the josephson tunnel current,” *Phys. Rev. Lett.*, vol. 11, pp. 200–202, Sep 1963.
- [8] S. M. Frolov, D. J. Van Harlingen, V. A. Oboznov, V. V. Bolginov, and V. V. Ryazanov, “Measurement of the current-phase relation of superconductor/ferromagnet/superconductor pi josephson junctions,” *Phys. Rev. B*, vol. 70, p. 144505, Oct 2004.
- [9] A. Assouline, C. Feuillet-Palma, N. Bergeal, T. Zhang, A. Mottaghizadeh, A. Zimmers, E. Lhuillier, M. Eddrie, P. Atkinson, M. Aprili, and H. Aubin, “Spin-orbit induced phase-shift in  $\text{Bi}_2\text{Se}_3$  josephson junctions,” *Nature Communications 2019 10:1*, vol. 10, pp. 1–8, 1 2019.
- [10] E. Strambini, A. Iorio, O. Durante, R. Citro, C. Sanz-Fernández, C. Guarcello, I. V. Tokatly, A. Braggio, M. Rocci, N. Ligato, V. Zannier, L. Sorba, F. S. Bergeret, and F. Giazotto, “A josephson phase battery,” *Nature Nanotechnology*.
- [11] M. J. A. Stoutimore, A. N. Rossolenko, V. V. Bolginov, V. A. Oboznov, A. Y. Rusanov, D. S. Baranov, N. Pugach, S. M. Frolov, V. V. Ryazanov, and D. J. V. Harlingen, “Second-harmonic current-phase relation in josephson junctions with ferromagnetic barriers,” 2018.
- [12] A. Pal, Z. Barber, J. Robinson, and M. Blamire, “Pure second harmonic current-phase relation in spin-filter josephson junctions,” *Nature Communications*, vol. 5, Feb. 2014.

- [13] Y. Tanaka and S. Kashiwaya, “Theory of josephson effects in anisotropic superconductors,” *Phys. Rev. B*, vol. 56, pp. 892–912, Jul 1997.
- [14] H. Sellier, C. Baraduc, F. Lefloch, and R. Calemczuk, “Half-integer shapiro steps at the 0-pi crossover of a ferromagnetic josephson junction,” *Phys. Rev. Lett.*, vol. 92, p. 257005, June 2004.
- [15] F. E. Schmidt, “Rcsj,” 2017.
- [16] “Achieving Accurate and Reliable Resistance Measurements in Low Power and Low Voltage Applications | Tektronix.”
- [17] D.-T. Ngo, “Lorentz tem characterisation of magnetic and physical structure of nanostructure magnetic thin films,” 12 2021.
- [18] L. Wang, “Fabrication stability of josephson junctions for superconducting qubits,” 2015.
- [19] T. Yamashita, K. Tanikawa, S. Takahashi, and S. Maekawa, “Superconducting  $\pi$  qubit with a ferromagnetic josephson junction,” *Phys. Rev. Lett.*, vol. 95, p. 097001, Aug 2005.
- [20] N. Klenov, V. Kornev, A. Vedyayev, N. Ryzhanova, N. Pugach, and T. Rumyantseva, “Examination of logic operations with silent phase qubit,” *Journal of Physics: Conference Series*, vol. 97, p. 012037, feb 2008.
- [21] J. A. Khan and M. Shahabuddin, “Simulation study of effect of magnetic field over i-v characteristic of intrinsic stacked josephson junctions,” *International Journal of Nanomanufacturing*, vol. 4, no. 1/2/3/4, p. 342, 2009.